RSC Advances

PAPER

View Article Online
View Journal | View Issue

Cite this: *RSC Adv.*, 2023, **13**, 33276

A novel carbazole-based fluorometric and colorimetric sensor for the highly sensitive and specific detection of Cu^{2+} in aqueous solution†

Yiduo Li, Luyue Wang, Liqiang Wang, Baokun Zhu and Jie Ma *

Received 9th July 2023
Accepted 2nd November 2023

DOI: 10.1039/d3ra04571d

rsc.li/rsc-advances

Based on the typical Suzuki coupling reaction and Schiff base reaction, a novel fluorescent molecular **PCBW** is synthesized and applied as a fluorescence and colorimetric sensor to detect Cu^{2+} in aqueous solution. The **PCBW** sensor presents the aggregation-caused quenching (ACQ) effect and at 1×10^{-5} mol L^{-1} it emits the strongest turquoise fluorescence in the DMSO–H_2O system (f_w = 40%). The sensor exhibits a 'turn-off' fluorescent characteristic by adding Cu^{2+}, and its fluorescent intensity shows a reliable linear relationship with the Cu^{2+} concentration in the range of 0–6×10^{-6} mol L^{-1}, with a detection limit of 1.19×10^{-8} mol L^{-1}. Meanwhile, the **PCBW** sensor also exhibits the colorimetric sensing from colorless to light yellow. The sensor has good selectivity and anti-interference and its pH application range can be extended from 5 to 10. The intramolecular charge transfer (ICT) is speculated as the main fluorescence mechanism of **PCBW**. In addition, the sensor presents good reusability and is practicable to detect Cu^{2+} in diverse aqueous samples.

1. Introduction

Copper is widely used in the machinery industry, wire industry, pipeline industry, and construction industry and it is also used in the auto parts industry. The widespread existence of copper and copper-containing substances makes Cu^{2+} an important metal pollutant.[1–3] Although copper is one of the necessary trace elements for the human body and plays an important role in various physiological processes of the human body, it will cause serious environmental pollution and harm to human health when it is in excess.[4,5] The abnormal concentrations of copper have been linked to several serious diseases,[6,7] such as Wilson's disease,[8] Alzheimer's disease,[9] Menkes syndrome,[10] Parkinson's disease,[11] and prion disease.[12] According to the World Health Organization (WHO), the standard of copper ion in drinking water has a median value of 23.4 μmol L^{-1} in the range of 0.78–46.9 μmol L^{-1}.[13] Therefore, it is a very important research point to develop a fast, sensitive, and reliable method to detect Cu^{2+} in diverse samples.

In past decades, various detection methods have been applied to detect Cu^{2+} ions in biological and environmental samples, such as atomic emission spectrometry (AES), mass spectrometry (MS), inductively coupled plasma spectroscopy (ICP), atomic absorption spectrometry (AAS), electrochemical methods, *etc.*[14–16] However, the above methods still have some disadvantages including complex and expensive instruments, complex detecting procedures, and long time-consuming, and off-site tests. Recently, a fluorescence method has been paid more attention due to its advantages of convenient operation, high selectivity and sensitivity, fast response time, low cost, *etc.*[17–20] So far, although many fluorescent sensors have been designed and developed to detect Cu^{2+},[21–24] with the increasing requirements for the environment and application of ion detection, the design and development of new fluorescent sensors is still a hot spot in the field of fluorescence detection.[25]

Carbazole is a kind of aromatic heterocyclic compound rich in electrons and an important intermediate of many fine chemicals. Commonly, the 3 and 6 positions of carbazole have high activity and can carry out a series of reactions, such as Friedel–Crafts alkylation, Friedel–Crafts acylation, nitration, halogenation formylation, and so on.[26] Many kinds of carbazole derivatives can be synthesized by the relative reaction modifying functional monomers, these carbazole derivatives with large conjugate systems may show high active electron transfer ability, high thermal stability, photochemical stability, photoelectric properties, and bioactivity properties.[27,28] They have been widely applied in many fields, such as photoelectric materials, chemical dyes, clinical medicine, molecular recognition, and so on.[29] In recent years, carbazole derivatives have been used as fluorophore moiety to construct fluorescent molecular sensors due to their large π-conjugated rigid planar structure and active intramolecular charge transfer characteristic.[30–32]

In this paper, a new type of coordinated fluorescent material named (2-hydroxyphenyl) {2-[(*E*)-[4-(9-phenylcarbazol-3-yl) phenyl] methylidene] diazanyl} methanone (**PCBW**) is synthesized successfully *via* two-step reactions. The **PCBW** molecule with a given concentration at 1×10^{-5} mol L^{-1} shows special

School of Materials and Chemistry, University of Shanghai for Science and Technology, Shanghai, 200093, P. R. China. E-mail: majie@usst.edu.cn; majie0203ch@hotmail.com

† Electronic supplementary information (ESI) available. See DOI: https://doi.org/10.1039/d3ra04571d

fluorescence properties at 477 nm in the mixed solution of DMSO–H_2O ($f_w = 40\%$). It shows a special "turn-off" fluorescent response for detecting Cu^{2+}. Meanwhile, Cu^{2+} will make the color of the **PCBW** solution change from colorless to light yellow in sunlight. The fluorescence intensity of **PCBW** at 477 nm shows a reliable linear relationship with the concentration of Cu^{2+}. In a given DMSO–H_2O system, the **PCBW** sensor shows excellent selectivity and anti-interference and has excellent reusability. The detection mechanism of **PCBW** is analyzed by high-resolution mass spectrometry (HRMS), nuclear magnetic resonance (NMR), and theoretical calculation. The reported method provides a good reference for constructing novel carbazole-based fluorescent sensors applied in different fields.

2. Experimental section

2.1. Materials and apparatus

All reagents are analytical grade without further purification in procedures except for some specific reagents specified. They are purchased from the Chemical Reagents Ltd. Co. of Sinopharm Group (China). All metal ions are provided by relatively soluble salts, including $CuCl_2 \cdot 2H_2O$, $AgNO_3$, $Co(NO_3)_2 \cdot 6H_2O$, $ZnCl_2$, $Pb(NO_3)_2$, $AlCl_3 \cdot 6H_2O$, $CdCl_2$, $CrCl_3$, $MnCl_2$, $FeCl_3 \cdot 6H_2O$, $NiSO_4 \cdot 6H_2O$, $Hg(NO_3)_2$, KCl, NaCl, $CaCl_2$, $MgSO_4$, $BaCl_2 \cdot 2H_2O$. 3-Bromo-*N*-phenyl-9*H*-carbazole is purchased from Aladdin with 98% purity. 2-Hydroxybenzhydrazide is purchased from Aladdin with 98% purity.

High-resolution mass spectra (HRMS) are recorded with Thermo Scientific Q Exactive (Thermo Fisher-QE, America). LC-MS spectra are measured by a Liquid Chromatography-Mass Spectrometer (LCMS-2020, Japan). NMR spectra are recorded by an NMR spectrometer (Bruker AV-400, Germany). Monitoring fluorescence intensity by fluorescence spectrometer (FL-7000, Hitachi, Japan). The UV-vis spectrum is recorded on the UV-vis spectrophotometer (UV-3900, Hitachi, Japan). Particle size data recorded on a dynamic light scattering instrument (Dynapro Titan TC, Wyatt Technology, America).

2.2. Synthesis process

2.2.1 Synthesis of PCB. The intermediate **PCB** is synthesized *via* a typical Suzuki condensation reaction, shown in Scheme 1. 2.00 g 3-bromo-*N*-phenyl-9*H*-carbazole (compound **1**, 6.020 mmol) and 1.12 g 4-formylphenylboronic acid (7.469 mmol) are transferred successively into a three-neck flask and dissolved with 25 mL THF. 4.29 g K_2CO_3 (31.041 mmol) is dissolved in 17.5 mL distilled water and the solution is transferred to the three-neck flask. 120 mg triphenylphosphine palladium ($Pd(PPh_3)_4$) is rapidly added into the flask under nitrogen protection, and then the flask is refluxed at 65 °C for 14 h under magnetic stirring. After thin-layer chromatography (TLC) monitoring, the product is extracted three times with 30 mL dichloromethane (DCM) and distilled water, then the organic phase is collected and evaporated to obtain a dry crude sample. Finally, the crude sample is purified by column

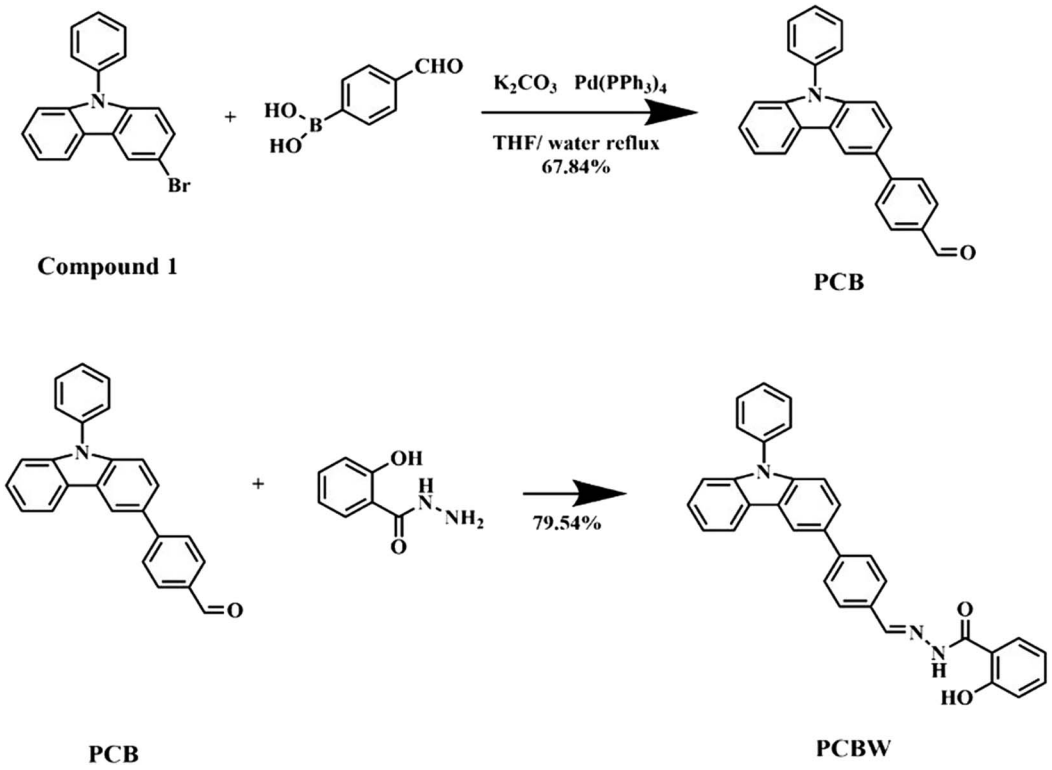

Scheme 1 The synthetic route of the sensor PCBW.

chromatography on silica gel (10 : 1 PE–EA) and the pure white solid 4-(9-phenylcarbazol-3-yl)benzene-1-carbaldehyde (**PCB**) is obtained (1.4653 g, yield 67.84%). ^{1}H NMR (600 MHz, DMSO-d_6) δ 10.05 (s, 1H), 8.74 (d, J = 1.6 Hz, 1H), 8.38 (d, J = 7.7 Hz, 1H), 8.02 (q, J = 8.3 Hz, 4H), 7.84 (dd, J = 8.6, 1.7 Hz, 1H), 7.70 (t, J = 7.7 Hz, 2H), 7.64 (d, J = 7.4 Hz, 2H), 7.56 (t, J = 7.4 Hz, 1H), 7.45 (dd, J = 7.9, 4.9 Hz, 2H), 7.39 (d, J = 8.2 Hz, 1H), 7.33 (t, J = 7.4 Hz, 1H). ^{13}C NMR (126 MHz, DMSO-d_6) δ 192.41, 146.39, 140.54, 140.10, 136.43, 134.23, 130.61, 130.06, 130.02, 127.69, 126.94, 126.48, 125.30, 123.35, 122.67, 120.75, 120.23, 119.19, 110.02, 109.64. LC-MS: purity 98%, m/z $[M + 1]^+$ 347.2 (calcd 347.2). ^{1}H NMR, ^{13}C NMR, and LC-MS spectra are listed in the ESI (Fig. S1–S3†).

2.2.2 Synthesis of PCBW. The **PCBW** is synthesized by a typical Schiff base reaction, shown in Scheme 1. 0.10 g **PCB** (0.287 mmol) and 0.06 g 2-hydroxybenzhydrazide (0.403 mmol) are added into the high-pressure tube and dissolved with 5 mL anhydrous ethanol; after two drops of acetic acid are added as a catalyst, the tube is stirred at 60 °C for 6 h. The product is extracted with ethyl acetate and distilled water three times. After some anhydrous sodium sulfate is added into the extracted solution to absorb the residual water for 1 hour, the extracted solution is evaporated to obtain a dry crude sample. Finally, the crude sample is purified by column chromatography on silica gel (6 : 1 PE–EA) and the pure white solid **PCBW** (0.1103 g, yield 79.57%) is obtained. ^{1}H NMR (600 MHz, DMSO-d_6) δ 11.90 (s, 1H), 11.89 (s, 1H), 8.71 (s, 1H), 8.53 (s, 1H), 8.39 (s, 2H), 7.95 (s, 1H), 7.94 (s, 1H), 7.89 (s, 2H), 7.86 (s, 1H), 7.84 (s, 1H), 7.72 (s, 1H), 7.68 (s, 2H), 7.57 (s, 1H), 7.47 (s, 2H), 7.42 (s, 1H), 7.34 (s, 1H), 7.01 (s, 1H), 6.99 (s, 1H), 6.98 (s, 1H). ^{13}C NMR (151 MHz, DMSO) δ 165.21, 159.52, 148.94, 142.95, 141.12, 140.39, 137.19, 134.30, 132.89, 131.95, 130.72, 129.08, 128.38, 127.47, 127.13, 125.68, 123.97, 123.38, 121.41, 120.79, 119.46, 119.26, 117.77, 116.45, 110.60, 110.26. HRMS: m/z $[M + 1]^+$ 482.2 (calcd 482.2). ^{1}H NMR, ^{13}C NMR, and HRMS spectra are listed in the ESI (Fig. S4–S6†).

2.3. Preparation of stock solutions and detecting solutions

The **PCBW** substance is fully dissolved in DMSO to prepare a concentration of 1×10^{-3} mol L^{-1} stock solution. The concentration of all investigated metal ions stock solution is also set as 1×10^{-3} mol L^{-1} with deionized water, including Cu^{2+}, Ag^{+}, Co^{2+}, Zn^{2+}, Pb^{2+}, Al^{3+}, Cd^{2+}, Cr^{3+}, Mn^{2+}, Fe^{3+}, Ni^{2+}, Hg^{2+}, K^{+}, Na^{+}, Ca^{2+}, Mg^{2+}, Ba^{2+}. All prepared stock solutions are fully oscillated evenly mixed and stored at room temperature (25 °C). The 1×10^{-3} mol L^{-1} EDTA stock solution is prepared from Na_2EDTA and deionized water. The **PCBW** sensors are set as 10 mL volume with the concentration of **PCBW** at 1×10^{-5} mol L^{-1} in the DMSO–H_2O system. For example, when a water content (f_w) is given at 40% (f_w = 40%), the sensor system is prepared from 0.1 mL **PCBW** stock solution, 0.1 mL metal ion stock solution, 5.9 mL DMSO solvent, and 3.9 mL deionized water. The UV absorption spectra of all analyte solutions are recorded in the range of 310–425 nm. The fluorescence emission spectra excited by 352 nm light are recorded in the range from 370 nm to 710 nm.

2.4. The pH experiments and the repeatability experiments

Since the probe is used for the detection of Cu^{2+} in solution, the optimum pH range of the tested solution is worth discussing. To study the stability of the probe in different pH samples, the solution is composed of 0.1 mL **PCBW** stock solution, 5.9 mL DMSO solvent, and 4.0 mL deionized water (pH = 2–12), then the fluorescence intensity of these probe solutions is measured in turn. For the ability of the **PCBW** probe to identify Cu^{2+} in different pH solutions, when water content is given at 40%, the sensor solution system is made from 0.1 mL **PCBW** stock solution, 5.9 mL DMSO solvent, 0.001 mL 0.1 mol per L Cu^{2+} stock solution and 3.999 mL deionized water (pH = 2–12) and then measure the fluorescence intensity of these prepared solutions.

All repeatability experiments are performed under the same conditions except for the addition of different amounts of Cu^{2+} and EDTA from their stock solutions (1×10^{-3} mol L^{-1}) alternately. The volume amounts of copper ions and EDTA stock solutions used in the 11 experiments are 0.1 mL Cu^{2+}, 0.1 mL Cu^{2+} + 0.1 mL EDTA, 0.2 mL Cu^{2+} + 0.1 mL EDTA, 0.2 mL Cu^{2+} + 0.2 mL EDTA, 0.3 mL Cu^{2+} + 0.2 mL EDTA, 0.3 mL Cu^{2+} + 0.3 mL EDTA, 0.4 mL Cu^{2+} + 0.3 mL EDTA, 0.4 mL Cu^{2+} + 0.4 mL EDTA, 0.5 mL Cu^{2+} + 0.4 mL EDTA, 0.5 mL Cu^{2+} + 0.5 mL EDTA, 0.6 mL Cu^{2+} + 0.5 mL EDTA in turn. The two storage solutions are added in a rotating order of 0.1 mL Cu^{2+} and 0.1 mL EDTA until the set amount.

2.5. Computational method

Simulation calculations about the monomolecular of **PCBW** are carried out in the Gaussian 09 software package based on DFT and TD-DFT theories. The DFT based on the B3LYP/6-31G* model is performed for the geometries of relative molecules. Based on the above, the lowest empty molecular orbital (LUMO) and highest occupied molecular orbital (HOMO) states and electron cloud distributions are calculated by M06-2X/6-31G* basis set.

3. Results and discussion

3.1. Effect of water content on the PCBW sensor

Due to **PCBW** not being soluble in water but in DMSO, a DMSO–H_2O mixture is used as its solvent to construct the sensor system. Fig. 1a shows the change curve of the fluorescence intensity of the **PCBW** sensor with different water content, excited by 352 nm UV light. It is indicated the **PCBW** sensor has the strongest fluorescence intensity when the water content is about 40%. As the water content increases by over 40%, the fluorescence intensity of the sensor gradually decreases from approximately 5500 a.u. to below 1000 a.u. However, when the water content increases from 0% to 40%, the fluorescence intensity of the sensor gradually increases, accompanied by a redshift. The above results indicate that water content is a critical factor for the **PCBW** fluorescent system. It should be attributed that **PCBW** molecules are concentrated and even aggregated with the increase of f_w. Fig. S11† is particle size of **PCBW** at different moisture contents detected by dynamic light scattering (DLS), demonstrates that as the water content

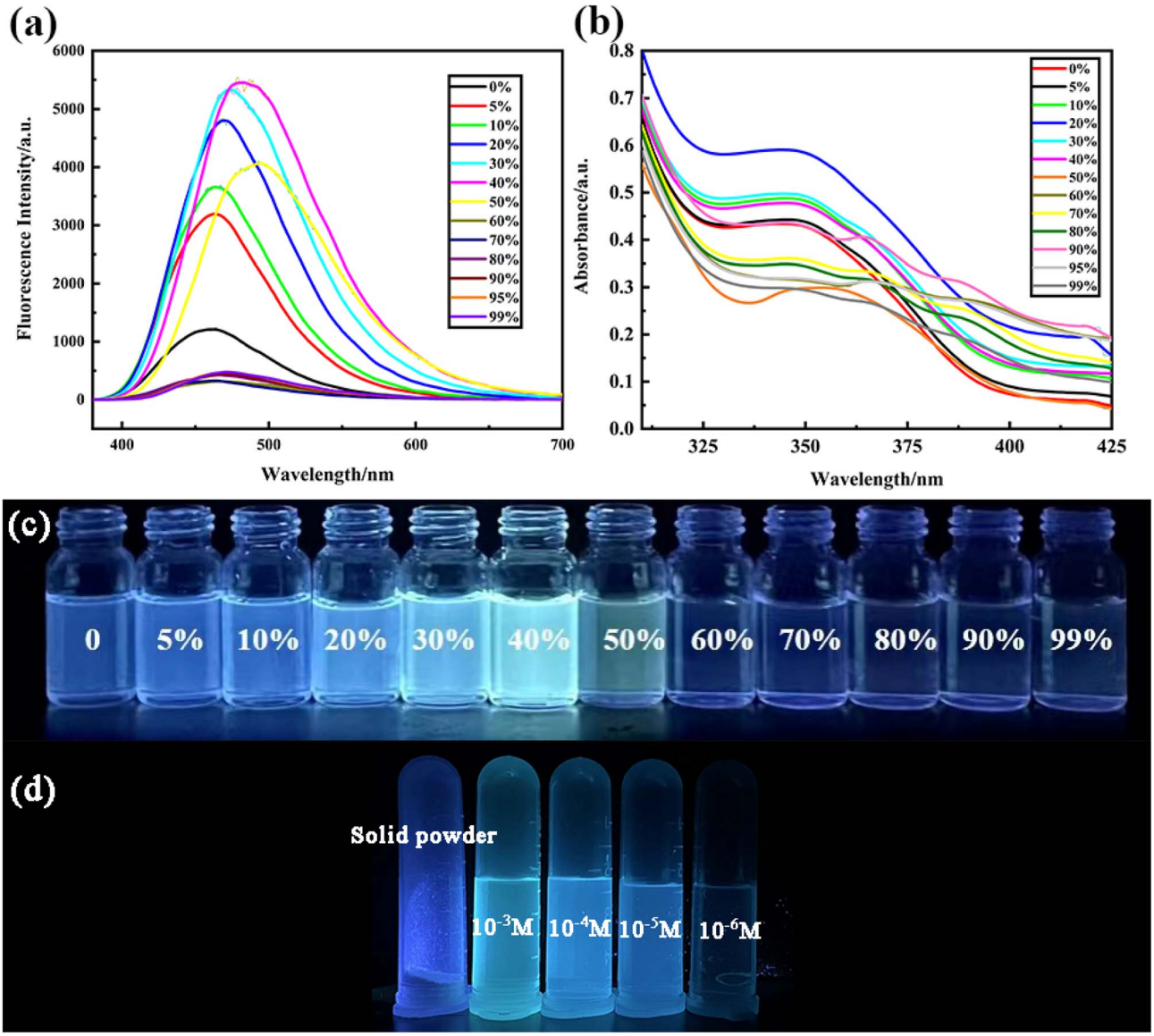

Fig. 1 (a) Fluorescence spectra of **PCBW** in DMSO–H_2O with different water content. (b) Their UV-vis spectra. (c) Their digital photographs were obtained under long wavelength UV lamp light. (d) Digital photographs of different concentrations of **PCBW** in DMSO solution obtained under long wavelength UV lamp light.

increases, the particle size in the system shows a trend of first increasing and then decreasing, and reaches its maximum at 60% water content. We speculate that within the range of 0–40%, the system can be seen as dominated by DMSO, with water molecules dissolved in DMSO; at 40–60%, water, and DMSO act as mutual solvents, because compound **PCBW** are insoluble in water and will exists in the system as DMSO–**PCBW** droplets, reaching its maximum at 60%; when the water content exceeds 60%, it can be seen as water as a solvent, and **PCBW**–DMSO droplets are dispersed in the aqueous phase. As the water content increases, DMSO in the droplets is forced to transfer to water, resulting in a continuous decrease in particle size, and the aggregation of molecule **PCBW**. As the concentration increases to a certain extent, its fluorescence intensity reaches the maximum; then fluorescence of the **PCBW** sensor decreases with the continuous increase in water content, due to the aggregation of molecules. Therefore, the synthesized **PCBW** should belong to ACQ fluorescent material; the red-shift phenomenon of fluorescence is attributed to the increase of decay of non-radiative transition energy caused by intermolecular interaction.

Fig. 1b and S9† are the ultraviolet absorption spectra of the **PCBW** sensor with different water content. The UV-vis absorption spectrum of the sensor has an obvious absorption band between 310–425 nm, and the position and intensity of the UV-vis absorption peak of **PCBW** are different under different water content. With the water content less than 40%, the sensor shows an absorption band in the range of 325 to 400 nm. However, the absorbing band is also widened and red-shifted with water content beyond 40%. The decrease in intensity

around 350 nanometers should be attributed to the interactions among aggregated molecules.

Fig. 1c shows a digital photograph of a **PCBW** sensor in different water content under long wavelength UV lamp light. It can be seen that the fluorescence intensity is the strongest with the water content of 40%, which is accordingly with the spectrum results shown in Fig. 1a. As shown in Fig. 1d, by varying the fluorescence intensity of **PCBW** at different concentrations in pure DMSO, it can be further confirmed that **PCBW** has an ACQ effect, as its solid does not emit fluorescence under long wavelength UV lamp light. It can also be demonstrated that there is a significant red shift in its fluorescence with its concentration increases. This result supports the speculation that adding water may lead to the concentration of **PCBW** in the DMSO–H_2O system.

It is speculated that the **PCBW** molecule will emit strong fluorescence in the suitable dispersed state. However, its exciton energy may be expended *via* a non-radiative route by the interaction among aggregated molecules, leading to a decrease or even disappearance of fluorescence intensity. To ensure the effectiveness of the experiment, the ideal **PCBW** sensor (1×10^{-5} mol L^{-1}) is constructed with the compound dispersed in a DMSO–H_2O solvent containing water 40% at room temperature (25 °C).

3.2. Selectivity and sensitivity of the PCBW sensor

To investigate the specificity of the **PCBW** sensor for Cu^{2+}, the fluorescence spectra and UV-vis absorption spectra changes of the probe with 17 kinds of ions are measured. These spectral analyses are carried out under the same condition except for different kinds of cations, including Ag^{+}, Co^{2+}, Zn^{2+}, Pb^{2+}, Al^{3+}, Cd^{2+}, Cr^{3+}, Mn^{2+}, Fe^{3+}, Ni^{2+}, Hg^{2+}, K^{+}, Na^{+}, Ca^{2+}, Mg^{2+}, Ba^{2+} ($[M]^{n+} = 1.0 \times 10^{-5}$ mol L^{-1}). It can be seen from the fluorescence spectra shown in Fig. 2a and the fluorescent image shown in Fig. 2d that only copper ions can cause fluorescence quenching of the probe, although other ions have slightly different effects on it. Meanwhile, the UV-vis absorption spectra shown in Fig. 2b and the daylight image shown in Fig. 2c further indicate that only copper ion can cause the change of the UV-

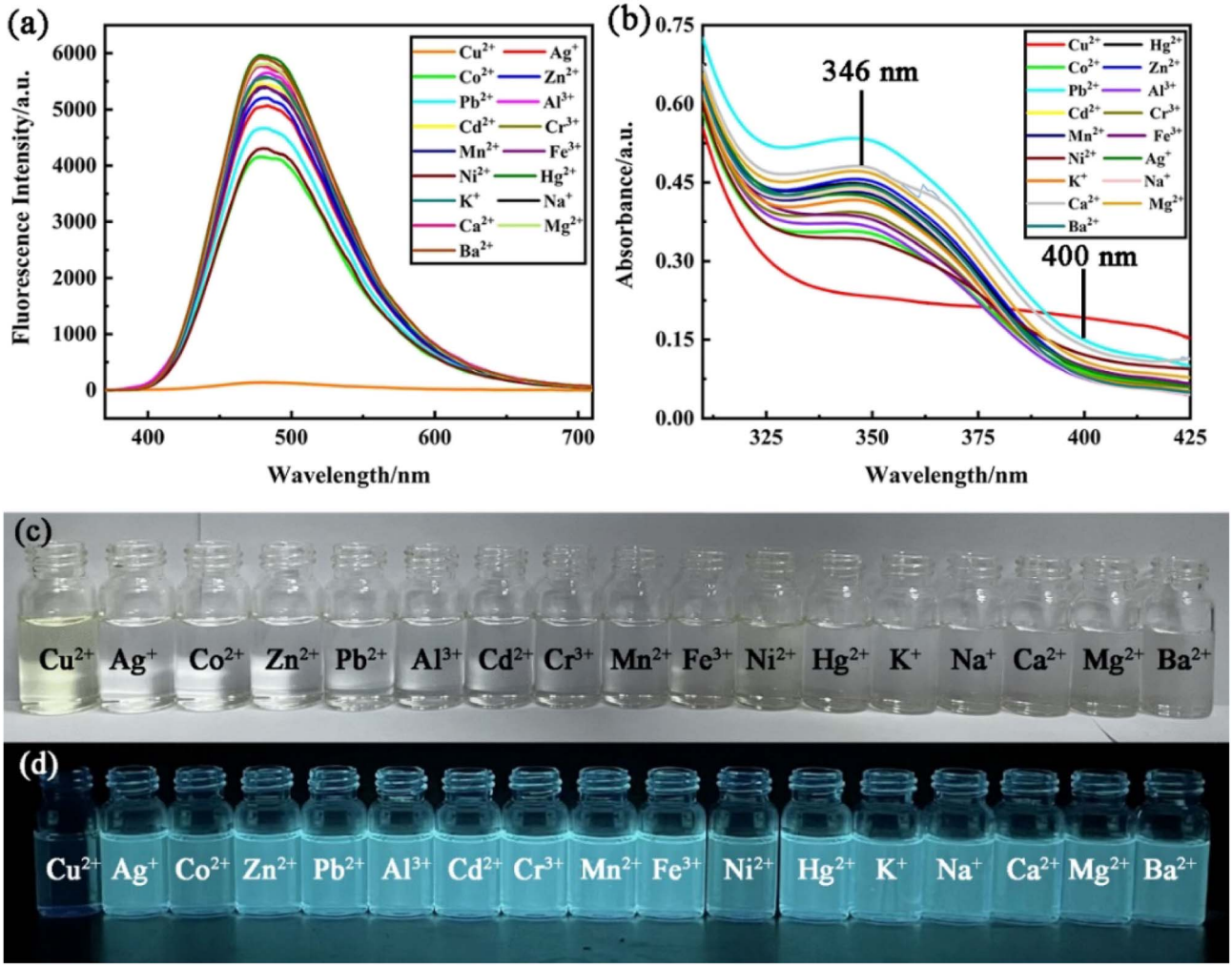

Fig. 2 (a) Fluorescence spectra of the **PCBW** sensor with various metal ions. (b) The UV-vis spectra of the **PCBW** sensor with metal ions. (c) Digital photograph of **PCBW** with metal ions under daylight. (d) Digital photograph of **PCBW** with metal ions under long wavelength UV lamp light.

visible absorption spectrum of the probe molecule. The above results indicate that the **PCBW** sensor has excellent specificity for copper ions in both fluorescent detection and colorimetric detection within the range of 17 ions examined. Digital photographs of **PCBW** interacting with metal ions under daylight and long wavelength UV lamp light are shown in Fig. 2c and d. It further indicates that after adding Cu^{2+}, **PCBW** solution is transparent light yellow under sunlight and non-fluorescence under long wavelength UV lamp light. Meanwhile, whether in sunlight or under long wavelength UV lamp light, the color of the probe system hardly changes with the addition of other ions. The specificity of the sensor should be attributed to the formation of **PCBW**–Cu^{2+} complexes *via* Cu^{2+} coordinating with N and O atoms in **PCBW** molecules, while other ions cannot form stable complexes, so it has little effect on its fluorescence and UV-visible absorption. The formation of copper ion and **PCBW** complex leads to the change of its probe molecular structure, which results in its fluorescence quenching. With the addition of copper ions, the UV visible absorption spectral band shifts from around 346 nanometers to the visible light region around 400 nanometers, resulting in the color of the solution changing from colorless to light yellow. Therefore, we can preliminarily determine if copper ions are present in the probe system by observing the color changes of the sensor system under natural light with the naked eye.

The anti-interference experiment results of the **PCBW** sensor are shown in Fig. 3. It shows the comparative data of the fluorescence intensity at 477 nm of the **PCBW** sensor after the addition of various ions in the presence or absence of copper ions. For comparison purposes, the fluorescence intensity of the blank sensor and the sensor adding copper ions is placed on the leftmost of the bar graph in Fig. 3. It is found that the fluorescence intensity of the **PCBW** sensor containing 16 cations is similar to that of the pure sensor when Cu^{2+} is absent, further indicating the sensor does not have recognizability to them. Meanwhile, the fluorescence of all **PCBW** sensors containing different cations is almost completely quenched in the presence of Cu^{2+}. These results prove that Cu^{2+} ions can effectively quench the fluorescence of the **PCBW** sensor and these metal ions hardly interfere with the detection of Cu^{2+} ions. These results further suggest that the constructed sensor has excellent specificity and anti-interference ability for detecting copper(II) ions in aqueous.

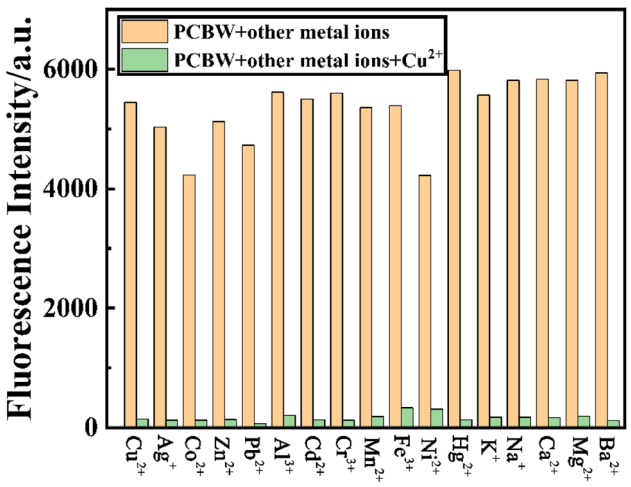

Fig. 3 The fluorescence intensity at 477 nm of **PCBW** sensor with diverse metal ions (1×10^{-5} mol L^{-1}) alone or with Cu^{2+} (1×10^{-5} mol L^{-1}).

3.3. Effect of Cu^{2+} concentration on the sensor

To study the fluorescence recognition ability of Cu^{2+}, a series of concentrations of Cu^{2+} are titrated into a given **PCBW** sensor system. The curve shown in Fig. 4a illustrates the change in fluorescence intensity of the sensor in the range of Cu^{2+} concentration from 0 to 1×10^{-5} mol L^{-1}. With the increase of Cu^{2+} concentration, the fluorescence emission peak of the **PCBW** sensor at 477 nm does not shift, but its intensity gradually decreases. The fluorescence intensity of the sensor at 477 nm shows a good negative linear with the concentration of Cu^{2+} in the range of 0–6×10^{-6} mol L^{-1}, and the fitting curve equation is as $y = -673.58x + 5404.26$ ($R^2 = 0.992$). It indicates that the **PCBW** sensor, as a fluorescence "turn-off" sensor, can be used for quantitative detection of Cu^{2+} content in the range of 0–6×10^{-6} mol L^{-1}. According to the equation as LOD = $3\sigma/s$ (σ represents the standard deviation of blank sample, s represents the absolute value of the coefficient of the fitting function between fluorescence intensity and the concentration of testing metal ion),[33] the LOD of the sensor reaches 1.19×10^{-8} mol L^{-1}, which further indicates the **PCBW** sensor has a good sensitivity for the detection of Cu^{2+} in solution. Meanwhile, the concentration of Cu^{2+} also can be roughly estimated *via* the naked eye by the fluorescence image obtained under long wavelength UV lamp light shown in Fig. S10.†

Fig. 4b shows the UV-visible spectrum of the sensor as a function of Cu^{2+} concentration from 0 to 1×10^{-5} mol L^{-1}. From the curves, it can be seen that as the concentration of copper ions in the system increases, the absorption peak intensity at 346 nm gradually decreases to a minimum, while the new absorption peak intensity at 400 nm gradually increases to a maximum. Due to the new absorption band from 400 nm to 425 nm belonging to the visible light region, the color of the **PCBW** sensor solution changes from colorless to faint yellow under sunlight (Fig. 2c). Therefore, it is possible to preliminarily determine the content of copper ions in the system by observing the color changes of the probe solution under sunlight with naked eyes. Moreover, the absorption intensity of the sensor at 400 nm also presents good positive linear with Cu^{2+} concentration in the range of 0–4×10^{-6} mol L^{-1}, and the fitting curve is as $y = 0.027x + 0.076$ ($R^2 = 0.998$). Therefore, according to the UV-vis absorption spectrum, the **PCBW** sensor can also quantitatively detect Cu^{2+} concentration in the range of 0–4×10^{-6} mol L^{-1}.

3.4. The presumed fluorescence detection mechanism

The coordination mechanism of the **PCBW** molecule with Cu^{2+} ion is studied by a series of Job's plot experiments. As shown in the following Fig. 5, when $[Cu^{2+}]:[Cu^{2+} + \textbf{PCBW}] \approx 1:3$, the

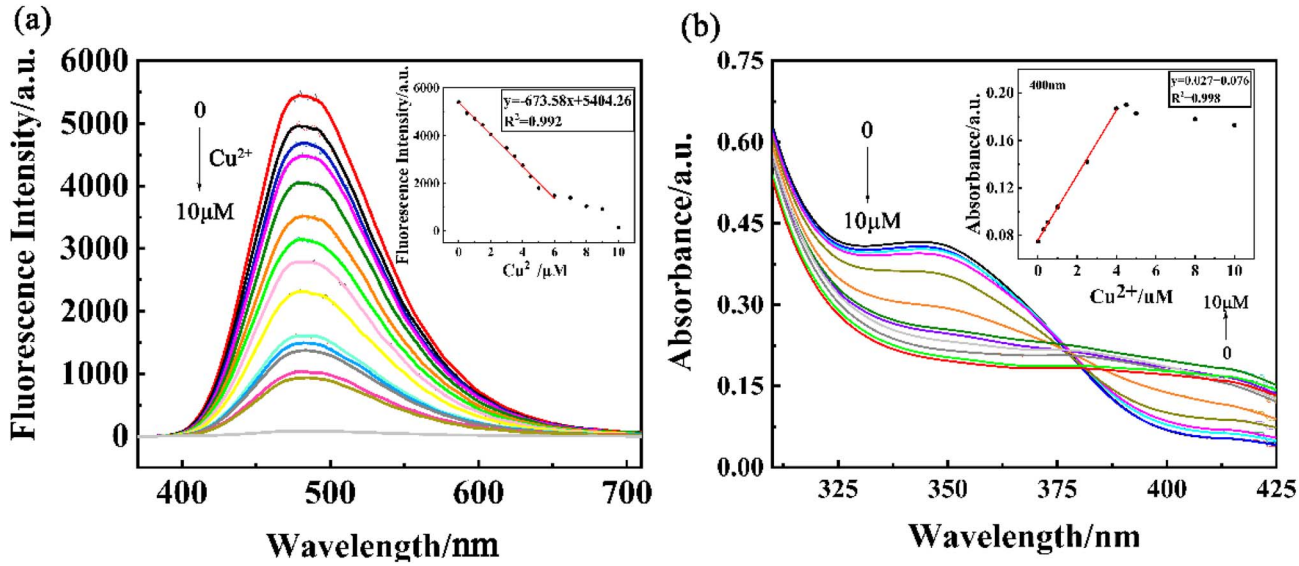

Fig. 4 (a) Fluorescence spectra of the sensor changed with Cu^{2+} from 0 to 1×10^{-5} mol L^{-1}, excited by 352 nm. The fitting curve of fluorescence intensity at 477 nm with Cu^{2+} concentration is inserted in it. (b) The UV-vis spectra of the sensor with the change of Cu^{2+} from 0 to 1×10^{-5} mol L^{-1}. The fitting curve of UV absorption intensity at 400 nm with Cu^{2+} concentration is inserted in it.

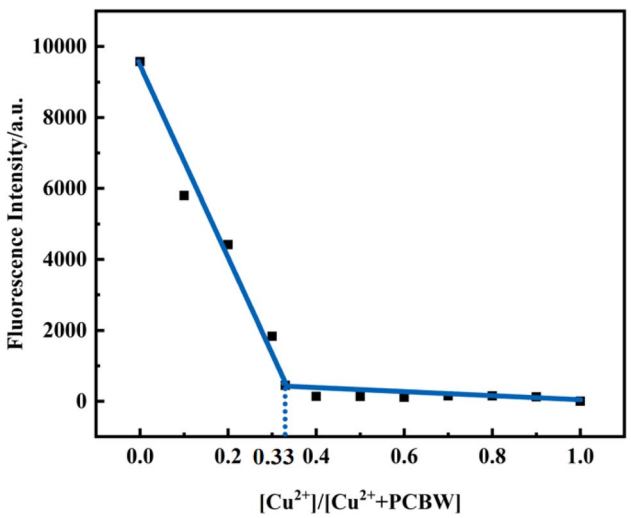

Fig. 5 Job's plot for **PCBW** molecule towards Cu^{2+} at 477 nm. The total concentration of **PCBW** and Cu^{2+} ions given at 2.5×10^{-5} mol.

fluorescence intensity is almost the lowest, indicating that the **PCBW** molecule coordinates with Cu^{2+} at a stoichiometric ratio of 2 : 1. The coordination mode of sensors **PCBW** and Cu^{2+} is deduced and proposed the possible coordination mode of sensors **PCBW** and Cu^{2+} as shown in Scheme 2. It is speculated that Cu^{2+} coordinates with the N atom of the imino group and the O atom of hydroxyl groups in **PCBW** molecules to form metal coordination complexes. The peak at 1045.24 belongs to the *m*/*z* of 2**PCBW**–Cu–Na is found in the HRMS spectrum of **PCBW**–Cu^{2+} shown in Fig. S7,† further suggesting the stoichiometric ratio of **PCBW** to Cu^{2+} is 2 : 1. The binding constants K_a is calculated by the benefit software and the relative result is shown in Fig. S8,† the K_d ($1/K_a$) is estimated at 2.56×10^{-5} M, indicating a strong coordination effect between copper ions and **PCBW** fluorescent molecules. Due to the strong coordination between Cu^{2+} and **PCBW**, the ICT effect in **PCBW** molecules is restrained, resulting in its fluorescence quenching.

3.5. Theoretical analysis

To reasonably explain the Cu^{2+} response behavior observed in the experiment, based on DFT and TD-DFT, the optimized structure, HOMO and LUMO states, and electron distribution of sensor **PCBW** are studied *via* Gaussian 09 software. B3LYP/6-31G* level is adopted in Gaussian operation. Fig. 6 shows the optimized molecular configuration of **PCBW** and their corresponding frontier molecular orbital energy levels. In the HOMO and LUMO of **PCBW**, the electron cloud HOMO is mainly distributed on the carbazole group of the **PCBW** unit, and the benzene ring connected to the carbazole group, LUMO is distributed on the benzene ring connected to the carbazole group and the coordination center. It can be seen that the distribution of the electron cloud has an obvious shift, this shows that there is an obvious ICT process in **PCBW**. Because Cu^{2+} may coordinate with N and O atoms in **PCBW** molecules. Coordination may lead to changes in the structure and energy distribution of **PCBW** molecules. The result is that the fluorescence of **PCBW** disappears, so Cu^{2+} can quench the fluorescence of the probe. It further proves that the proposed recognition mechanism is reasonable.

3.6. The time response of the sensor

The time response performance of the sensor to Cu^{2+} is investigated and the results are shown in Fig. 7. It clearly shows that the fluorescence signal of the pure sensor remains stable at the time of 0–25 min. When 1×10^{-5} mol per L Cu^{2+} is added to the sensor solution, the fluorescence intensity of the sensor

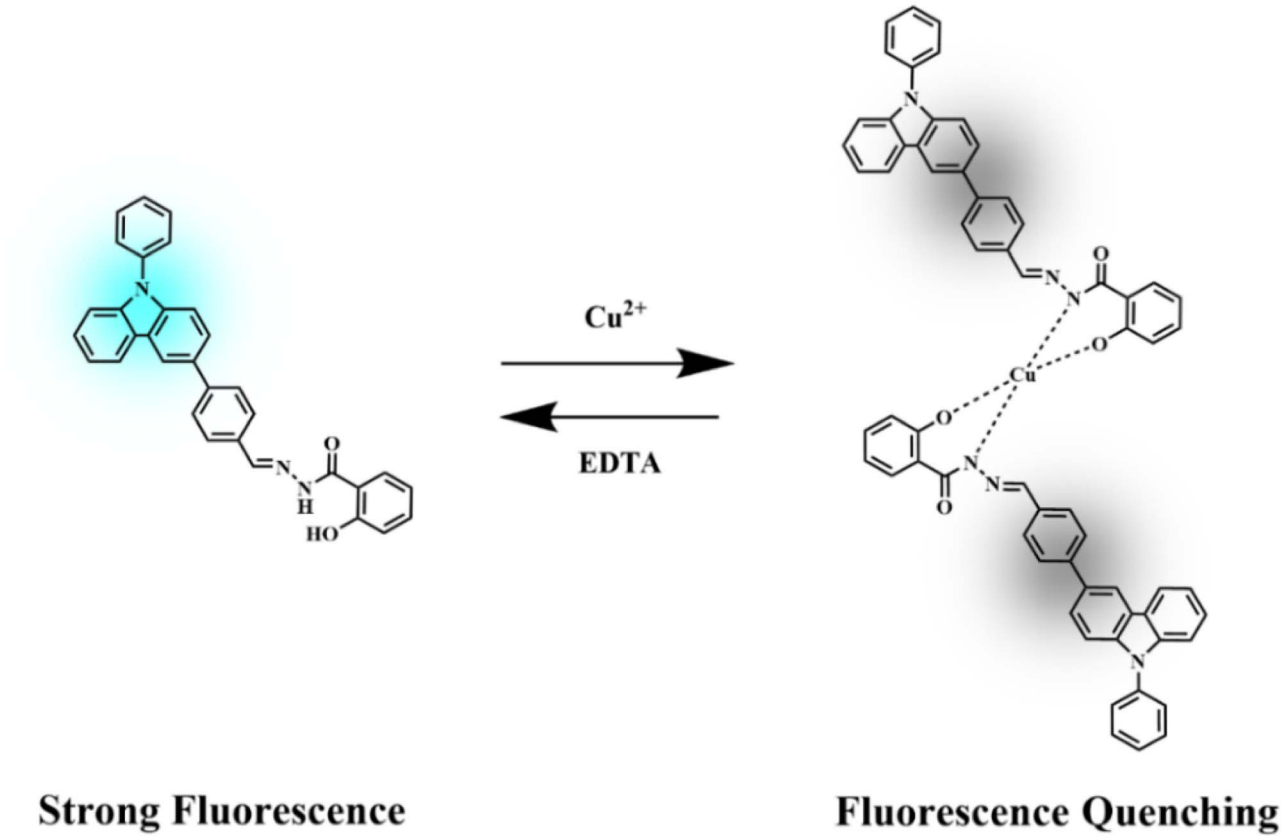

Scheme 2 A proposed binding mode between **PCBW** and Cu^{2+}.

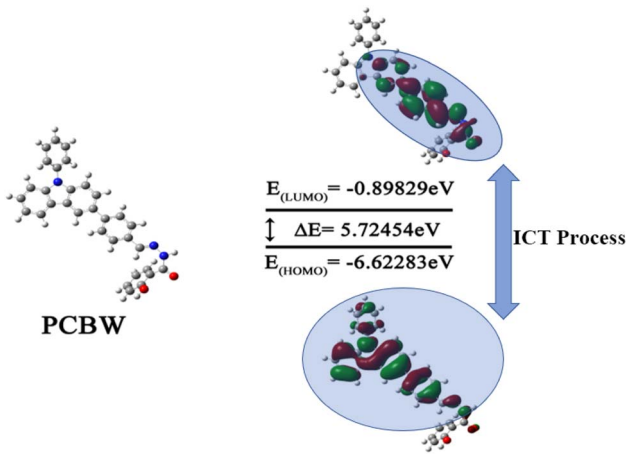

Fig. 6 HOMO and LUMO energy levels of **PCBW** with optimized structures.

immediately decreases, and then the fluorescence intensity of the sensor gradually decreases to the minimum for about 20 min and keeps stable. This phenomenon should be attributed to the different dissolution characteristics of **PCBW** and copper ions. The **PCBW** is wrapped in the DMSO organic phase while Cu^{2+} is dispersed in the water phase. The **PCBW** molecules on the surface of the organic phase immediately react with Cu^{2+}, so the fluorescence intensity of the sensor solution decreases immediately after adding Cu^{2+}. However, since the organic phase of the sensor, DMSO is 60% of the total system, and only the **PCBW** molecule on the surface can bind with Cu^{2+}, it takes a long time for copper ions to fully interact with fluorescent molecules. It shows that the sensor has good time response performance and can effectively detect Cu^{2+}.

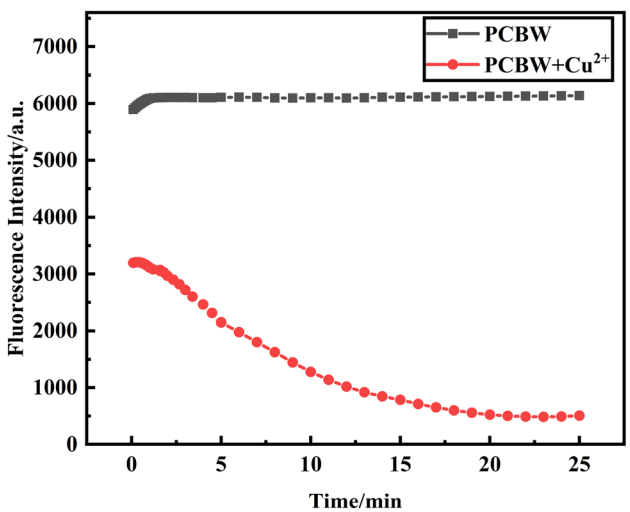

Fig. 7 Time-dependent fluorescence response at 477 nm of the **PCBW** sensor and the sensors in the presence of Cu^{2+}.

3.7. Applicable pH range of sensor

To study the optimum pH range of the sensor, we investigated the change of fluorescence intensity of the sensor in the pH range of 2 to 12 in the aqueous phase. It can be seen from Fig. 8 that the fluorescent intensity of the **PCBW** sensor increases when pH changes from 2 to 5; it then remains almost stable in the pH range of 5–10; finally, it decreases rapidly when pH exceeds 10. When equal amounts of copper ions are present in the sensor system, the fluorescence intensity of the system gradually decreases in the pH range of 2 to 5, and then it remains stable despite the pH ranging from 5 to 12. Indicating that the constructed **PCBW** sensor can effectively monitor copper ions in the pH range of 5–10. Because the pH value of real water samples is mostly within the range of 5–10, it indicates that the sensor has a broad prospect for Cu^{2+} detection in actual aqueous.

3.8. The recycling ability of the sensor

Reusability is one of the important indicators for evaluating coordination-type sensors. Therefore, EDTA, as a common ligand, is used to evaluate the reversibility of the **PCBW** sensor in detecting the procedure of Cu^{2+}. As shown in Fig. 9, the fluorescence of the **PCBW** sensor shows evident quench when an equal amount of Cu^{2+} is added to it. Then, with the addition of equimolar EDTA, the fluorescence emission intensity is significantly enhanced to its original value, indicating the as-prepared probe can be readily regenerated by EDTA. Subsequently, the alternating addition of Cu^{2+} and EDTA leads to fluorescence quenching and fluorescence recovery alternately. According to coordination theory, the reusability of the sensor should be attributed to the binding ability of EDTA to Cu^{2+} being stronger than that of **PCBW** to Cu^{2+}. When EDTA is added, EDTA molecules preferentially coordinate with Cu^{2+}, leading to the release of **PCBW** molecules from the **PCBW**–Cu^{2+} complex and the re-emergence of fluorescence. The reversible cycle is repeated at least 5 times, and there is only a small change in fluorescence intensity. Although the addition of EDTA one time can verify the recovery of the probe, it cannot indicate whether the presence of EDTA will interfere with the detection of copper ions. From these cyclic tests, it can be seen that when an equal amount of EDTA is added to Cu^{2+}, Cu^{2+} almost completely coordinate with EDTA, which is attributed to the huge difference in the coordination ability of probe molecules compared to EDTA. However, regardless of the content of EDTA, as long as the Cu^{2+} content exceeds EDTA, the **PCBW** probe has good sensitivity to Cu^{2+}. Therefore, during the testing process, adding copper ions equivalent to EDTA can eliminate the influence of the ligand on the probe, indicating the **PCBW** probe has good reusability and stability in high concentrations of EDTA conditions.

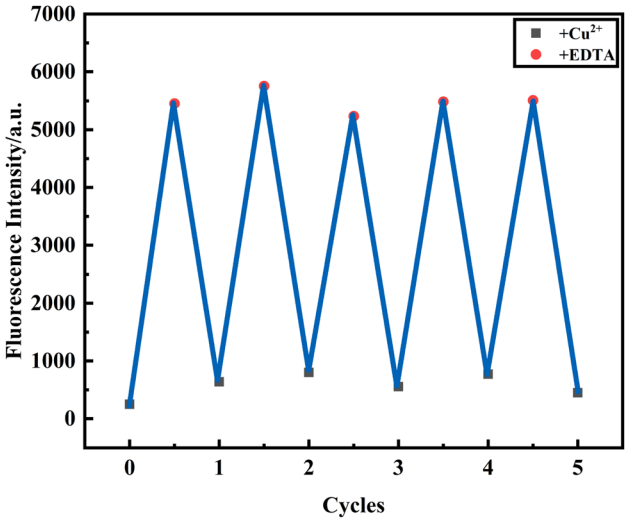

Fig. 9 Reversible changes of fluorescence intensity at 477 nm of PCBW upon addition of Cu^{2+} and EDTA alternately.

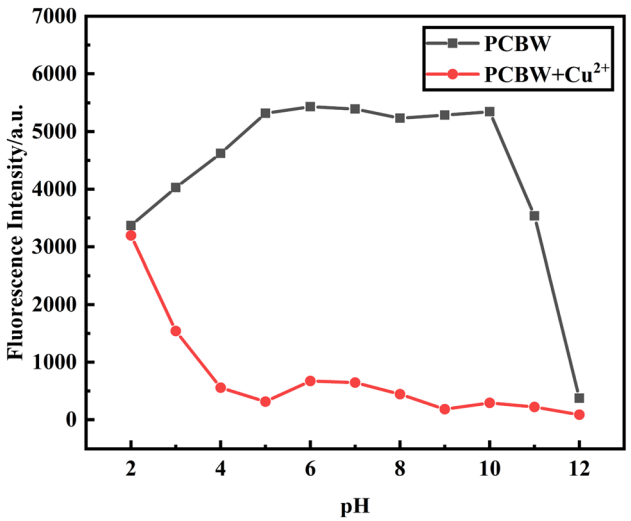

Fig. 8 The fluorescence intensity change at 477 nm of the PCBW sensor and the sensors in the presence of Cu^{2+} with different pH at 477 nm.

3.9. Application in real water samples

To explore the application of the **PCBW** sensor in real water samples, the fluorescence characteristics of the sensor for detecting Cu^{2+} are investigated in three real samples taken from tap water (from the Lab), mineral water (from Nongfu Spring), and river water (from Fuxing River), and all experimental conditions are same as those of the sensor taken from deionized water. Fig. 10 shows the linear fitting curve of the fluorescence intensity of four different water samples at 477 nm with the variation of Cu^{2+} concentration (scatter points represent the fluorescence intensity at 477 nm of four different water samples after adding different concentrations of Cu^{2+}. The four straight lines are the linear fitting curves of the fluorescence intensities of the four water samples). It presents that the fluorescence intensity of these **PCBW** sensors all decreases with the increase of Cu^{2+} concentration and they have a good linear relationship. Meanwhile, the fluorescence intensity of the sensor in a real water sample is lower than that in deionized water at the same conditions, indicating there is a trace amount of copper ion

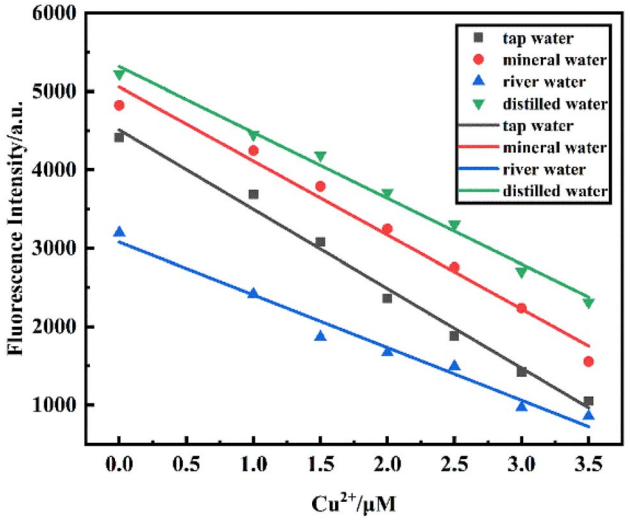

Fig. 10 The fluorescent intensity of **PCBW** with Cu^{2+} concentration of 0–3.5 × 10^{-6} mol L^{-1} in diverse real water samples (points and straight lines represent fluorescence intensity and fitting curve, respectively).

Cu^{2+} in real aqueous. The content of Cu^{2+} in a river is the highest among the three real water samples. Although these three types of water samples may contain a variety of complex ions and minerals, these substances hardly affect the sensor's determination of copper ions.

Based on the fitting curve ($y = -943.58x + 5056.73$) obtained in deionized water, the detection deviations of different concentrations of Cu^{2+} in tap water, mineral water, and river water are calculated, which are listed in Table 1. These results also show that Cu^{2+} exists in three actual water systems: tap water, mineral water, and river water. The concentrations of Cu^{2+} in tap water, mineral water, and river water are calculated to be 1.08 × 10^{-6} mol L^{-1}, 0.59 × 10^{-6} mol L^{-1} and 2.52 × 10^{-6} mol L^{-1}, in turn. The LOD of the **PCBW** sensor reaches 7.91 × 10^{-9} mol L^{-1}, 7.21 × 10^{-9} mol L^{-1} and 1.20 × 10^{-8} mol L^{-1} to detect Cu^{2+} in tap water, mineral water and river water, respectively, it can be seen that the detection limit of the probe for Cu^{2+} in tap water and mineral water is lower than that in deionized water. It shows that the prepared **PCBW** sensor can be well used for the detection of Cu^{2+} in real water, and has a wide application prospect.

3.10. PCBW-based test strips for Cu^{2+} detection

Fluorescent strip detection is a convenient, rapid, and efficient method for the detection of Cu^{2+}. It is easy to operate and suitable for real-time detection of real water. The filter paper is dripped by applying 1 × 10^{-3} mol per L **PCBW** solution and dried. During the test, 1 × 10^{-3} mol L^{-1} aqueous solution of metal ions is dropped on the test paper. Fig. 11 shows the photographs of **PCBW**-based test strips upon the addition of Na^{+}, Hg^{2+}, Cd^{2+}, Cr^{3+}, Ni^{2+}, and Cu^{2+} under sunlight and long wavelength UV lamp light. It can be seen that after adding metal ions under the sunlight, the color of the test strip remains the color of the original filter paper (white). Under the long wavelength UV lamp light, the test strip shows turquoise fluorescence with a metal ion solution other than Cu^{2+} is added, the color of fluorescence is the same as the test strip with only the pure sensor. Only the turquoise fluorescence of the test strip disappeared after adding Cu^{2+} and showing a black shadow. It is worth noting that the test paper dripped with Ni^{2+} also shows a perceptible black shadow, which is the same as the results of the previous selective experiment shown in Fig. 2a and d. It is worth noting that the **PCBW** solid has no fluorescence, but it emits bright turquoise fluorescence after being made into a dry test strip. This phenomenon should be attributed to the inability of **PCBW** molecules to aggregate in large quantities after dropping onto the test paper. It further indicates that the **PCBW** has an ACQ effect and its' test paper can qualitatively detect Cu^{2+} in aqueous.

Table 1 The content of Cu^{2+} in diverse real water samples monitored by PCBW probe and its deviation

Sample	Cu^{2+} spiked (1 × 10^{-6} mol L^{-1})	Cu^{2+} found (1 × 10^{-6} mol L^{-1})	Deviation (%)
Tap water	0	1.08	None
	1	1.94	86.0
	1.5	2.67	106.0
	2	3.52	122.0
	2.5	4.09	120.4
	3	4.64	118.7
	3.5	5.08	114.3
Mineral water	0	0.59	None
	1	1.28	69.0
	1.5	1.82	82.0
	2	2.47	94.0
	2.5	3.05	98.4
	3	3.67	102.7
	3.5	4.48	111.1
River water	0	2.52	None
	1	3.45	93.0
	1.5	4.10	105.3
	2	4.34	91.0
	2.5	4.55	81.2
	3	5.18	88.7
	3.5	5.32	80.0

3.11. Comparison of sensor PCBW with other reported fluorescence sensors for Cu^{2+} detection

According to Table 2, the detection limit of **PCBW** for Cu^{2+} recognition is lower than that of most fluorescent sensors previously reported. Many sensors need to be used under a specific pH, so it is necessary to use a buffer solvent (such as HEPES) to adjust the pH of the sensor solution before use, which not only complicates the operation but also increases the use of the buffer solution, while the sensor **PCBW** can effectively detect Cu^{2+} in a wide pH range of 5–10. There is no need to adjust the pH value of the solution when using sensor **PCBW** to detect Cu^{2+}. In addition, the sensor **PCBW** requires DMSO as a solvent, which is a relatively safe solvent, but most sensors use toxic reagents as solvents, such as THF, ACE, CH_3CN, *etc.* More importantly, although the sensor has an ACQ effect, it is suitable for use in a system with a water content of 40%, which is a relatively high-water system, such a system can reduce the use of organic solvents and be environmentally friendly.

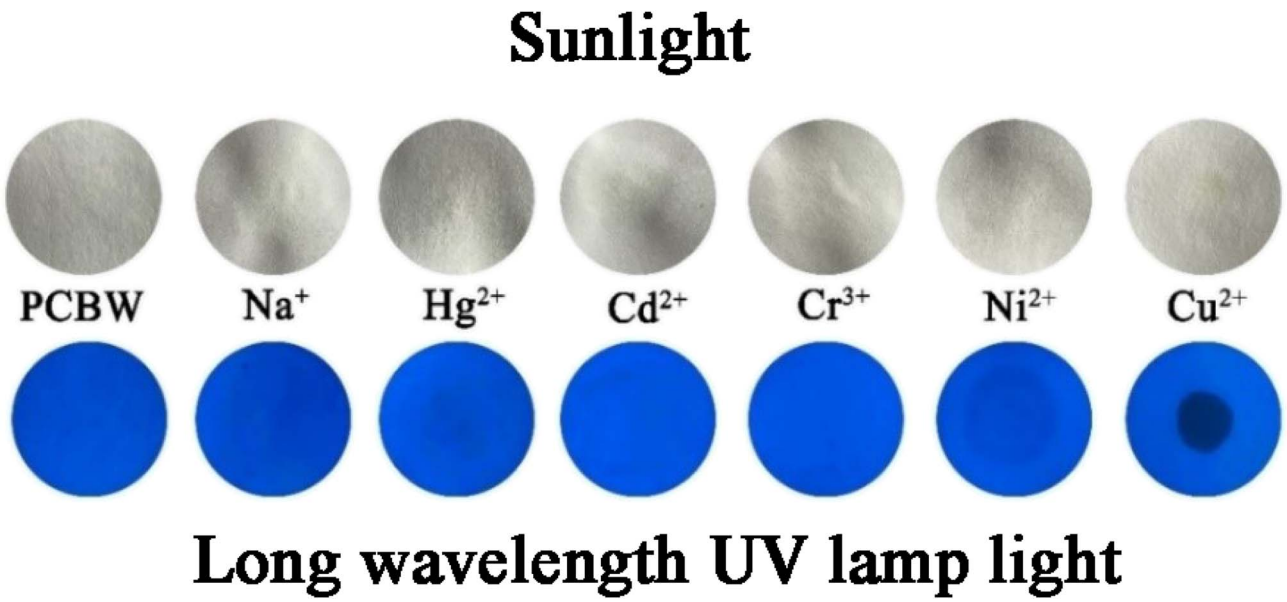

Fig. 11 The photographs of **PCBW**-based test strips upon addition of Na^+, Hg^{2+}, Cd^{2+}, Cr^{3+}, Ni^{2+}, and Cu^{2+} under sunlight and long wavelength UV lamp light.

Table 2 Comparison of **PCBW** with other reported fluorescence sensors

Sensor	Solution systems	LOD	Ref.
PCBW	DMSO/H_2O (6 : 4, v/v, pH = 5–10)	1.19×10^{-8} M	This work
HBT-H	ACE/H_2O (4 : 6, v/v, pH = 7.4)	3.08×10^{-7} M	34
AH	CH_3CN/H_2O (1 : 1, v/v, pH = 7.4)	4.22×10^{-8} M	35
TPE-1	THF/HEPES (1 : 9, v/v, pH = 7.3)	9.91×10^{-8} M	36
WGB	CH_3CN/HEPES (1 : 1, v/v, pH = 7.4)	6.76×10^{-8} M	37
BTN	CH_3CN	3.3×10^{-6} M	38
HMAN	CH_3CN/HEPES (95 : 5, v/v)	2.45×10^{-8} M	39
NPPY	DMSO/HEPES (95 : 5, v/v)	3.29×10^{-8} M	40
SH	DMSO/HEPES (95 : 5, v/v)	3.74×10^{-6} M	41
DA	DMSO/H_2O (1 : 1, v/v)	9.79×10^{-7} M	42
L	EtOH : HEPES (5 : 95, v/v)	5.31×10^{-7} M	43

4. Conclusions

In conclusion, a new **PCBW** molecule with ACQ effect is successfully synthesized. The **PCBW** sensor is constructed readily in the DMSO–H_2O system (f_w = 40%) at room temperature. As a turn-off fluorescence and colorimetric sensor, **PCBW** shows excellent selectivity, sensitivity, and anti-interference for detecting Cu^{2+} among 17 tested ions. The detection limit of the sensor reaches 1.19×10^{-8} mol L^{-1}. The fluorescence detection mechanism should be attributed to the formation of the **PCBW**–Cu^{2+} complex, and the fluorescence emission mechanism of the **PCBW** molecule belongs to the ICT effect according to the theoretical simulation results. With the presence of copper ion, the **PCBW**–Cu^{2+} complex is formed and the ICT effect is destroyed, resulting in the fluorescence quenching. The **PCBW** sensor has excellent reusability, which can be readily recovered by EDTA. The sensor shows effective application in the detection of Cu^{2+} in real water samples, and the strip containing **PCBW** can also be successfully applied to the detection of Cu^{2+}. The work provides an alternative thread for the synthesis of fluorescent molecules with AIE or ACQ effect based on the same fluorescent group through the modification of substituted moieties. Meanwhile, it is a good reference for the development and application of fluorescent sensors in the aqueous detection field.

Data availability

The data used or analyzed during the current study are available from the corresponding author upon reasonable request.

Author contributions

Yiduo Li and Jie Ma provided the initial idea for this work; Jie Ma, as supervisor, provided support; Luyue Wang, Liqiang Wang, and Baokun Zhu contributed to the collection and analysis of test data; Yiduo Li contributed to the theoretical calculation. Jie Ma and Yiduo Li contributed to the paper writing.

Conflicts of interest

The authors declare no interest or biases in the submitted work.

Acknowledgements

This work is financially supported by the Natural Science Foundation of Shanghai (No. 15ZR1428500). The authors are thankful to Haoyang Wang for the HR-ESI-MS analysis from the Shanghai Institute of Organic Chemistry, Chinese Academy of Sciences, and Chunfang Zheng for the HRMS analysis from Shiyanjia Lab (**https://www.shiyanjia.com**).

References

1 D. Udhayakumari, S. Naha and S. Velmathi, *Anal. Methods*, 2017, **9**, 552–578.
2 Y. Wang, X. H. Hao, L. X. Liang, L. Y. Gao, X. M. Ren, Y. G. Wu and H. C. Zhao, *RSC Adv.*, 2020, **10**, 6109–6113.
3 Y. P. Zhang, Y. C. Zhao, Q. H. Xue, Y. S. Yang, H. C. Guo and J. J. Xue, *Inorg. Chem. Commun.*, 2021, **129**, 108612.
4 J. Y. Shang, Y. B. Li, K. N. Chen and H. P. Li, *Chem. Pap.*, 2021, **75**, 1851–1859.
5 X. L. Niu, H. Zhang, X. J. Wu, S. B. Zhu, Y. L. Liu and M. Tian, *J. Mol. Struct.*, 2022, **1264**, 133294.
6 L. Huang, F. P. Hou, P. X. Xi, D. C. Bai, M. Xu, Z. P. Li, G. G. Xie, Y. J. Shi, H. Y. Liu and Z. Z. Zeng, *J. Inorg. Biochem.*, 2011, **105**, 800–805.
7 V. Desai and S. G. Kaler, *Am. J. Clin. Nutr.*, 2008, **88**, 855S–858S.
8 S. Lutsenko, *Biochem. Soc. Trans.*, 2008, **36**, 1233–1238.
9 M. G. Savelieff, S. Lee, Y. Z. Liu and M. H. Lim, *ACS Chem. Biol.*, 2013, **8**, 856–865.
10 B. E. Ziegler, R. A. Marta, M. B. Burt and T. B. McMahon, *Inorg. Chem. Commun.*, 2014, **53**, 2349–2351.
11 W. I. M. Vonk, V. Kakkar, P. Bartuzi, D. Jaarsma, R. Berger, M. H. Hofker, L. W. J. Klomp, C. Wijmenga, H. H. Kampinga and B. van de Sluis, *PLoS One*, 2014, **9**, e92408.
12 A. J. McDonald, J. P. Dibble, E. G. B. Evans and G. L. Millhauser, *J. Biol. Chem.*, 2014, **289**, 803–813.
13 A. A. Taylor, J. S. Tsuji, M. R. Garry, M. E. McArdle, W. L. Goodfellow, W. J. Adams and C. A. Menzie, *Environ. Manage.*, 2020, **65**, 131–159.
14 S. Feng, Q. Gao, X. Gao, J. Yin and Y. Jiao, *Inorg. Chem. Commun.*, 2019, **102**, 51–56.
15 L. Hou, J. Feng, Y. Wang, C. Dong, S. Shuang and Y. Wang, *Sens. Actuators, B*, 2017, **247**, 451–460.
16 Y. Qian, J. Lin, T. Liu and H. Zhu, *Talanta*, 2015, **132**, 727–732.
17 D. J. Zhu, A. S. Ren, X. C. He, Y. H. Luo, Z. H. Duan, X. W. Yan, Y. H. Xiong and X. Zhong, *Sens. Actuators, B*, 2017, **252**, 134–141.
18 Y. Liu, B. Jiang, L. L. Zhao, L. Zhao, Q. Y. Wang, C. Wang and B. C. Xu, *Spectrochim. Acta, Part A*, 2021, **261**, 120009.
19 X. D. Zeng, S. Gao, C. Jiang, Q. X. Duan, M. S. Ma, Z. G. Liu and J. Chen, *Luminescence*, 2021, **36**, 1761–1766.
20 Z. Q. Guo, Q. F. Wang, D. G. Zhou, Y. An, P. Wang and F. Liao, *Spectrochim. Acta, Part A*, 2022, **264**, 120257.
21 M. A. Assiri, A. G. Al-Sehemi and M. Pannipara, *Inorg. Chem. Commun.*, 2019, **99**, 11–15.
22 A. G. Al-Sehemi, A. Irfan, M. Pannipara, M. A. Assiri and A. Kalam, *Z. Phys. Chem.*, 2019, **233**, 895–911.
23 S. J. Jiang, J. B. Qiu, S. B. Chen, H. Y. Guo and F. F. Yang, *Spectrochim. Acta, Part A*, 2020, **227**, 117568.
24 X. D. Zeng, S. Gao, C. Jiang, X. Jin, M. S. Ma, Z. G. Liu and J. Chen, *Chemistryselect*, 2021, **6**, 6619–6624.
25 J. T. Yang, J. Chai, B. S. Yang and B. Liu, *Spectrochim. Acta, Part A*, 2019, **211**, 272–279.
26 V. Nayana and B. Kandasubramanian, *J. Polym. Res.*, 2020, **27**, 285.
27 A. K. Mitra, *J. Iran. Chem. Soc.*, 2022, **19**, 2075–2113.
28 F. Bekkar, F. Bettahar, I. Moreno, R. Meghabar, M. Hamadouche, E. Hernaez, J. L. Vilas-Vilela and L. Ruiz-Rubio, *Polymers*, 2020, **12**, 2227.
29 D. Erdener and I. Kaya, *J. Fluoresc.*, 2022, **32**, 2097–2106.
30 D. Li, S. Tu, Y. Le, Y. Zhou, L. Yang, Y. Y. Ding, L. Huang and L. Liu, *Spectrochim. Acta, Part A*, 2023, **285**, 121816.
31 H. F. Wang, P. P. Wang, L. F. Niu, C. H. Liu, Y. Z. Xiao, Y. Tang and Y. Chen, *Spectrochim. Acta, Part A*, 2022, **278**, 121257.
32 Y. Y. Zhu, R. Jia, Z. Y. Ke, X. W. Wang, L. P. Su, Y. P. Tian and X. H. Tian, *Dyes Pigm.*, 2022, **208**, 110875.
33 J. Pan, J. Ma, L. Liu, D. Li, Y. Huo and H. Liu, *J. Photochem. Photobiol., A*, 2021, **416**, 113322.
34 L. X. Zhao, K. Y. Chen, K. B. Xie, J. J. Hu, M. Y. Deng, Y. L. Zou, S. A. Gao, Y. Fu and F. Ye, *Dyes Pigm.*, 2023, **210**, 110943.
35 J. Y. Yang, W. Y. Gao, J. H. Wang, Z. M. Dong, Y. Wang and S. M. Shuang, *J. Lumin.*, 2023, **254**, 119549.
36 Y. X. Pan, Y. Li, X. F. Sun, L. J. Tang and X. M. Yan, *Dyes Pigm.*, 2023, **210**, 110985.
37 C. Segura, O. Yanez, A. Galdamez, V. Tapia, M. T. Nunez, I. Osorio-Roman, C. Garcia and O. Garcia-Beltran, *J. Photochem. Photobiol., A*, 2023, **434**, 114278.
38 G. Kim, D. Choi and C. Kim, *J. Fluoresc.*, 2021, **31**, 1203–1209.
39 F. N. Arslan, G. A. Geyik, K. Koran, F. Ozen, D. Aydin, S. N. K. Elmas, A. O. Gorgulu and I. Yilmaz, *J. Fluoresc.*, 2020, **30**, 317–327.
40 V. Bhardwaj, S. K. A. Kumar and S. K. Sahoo, *Microchem. J.*, 2022, **178**, 107404.
41 D. A. Patel, S. K. A. Kumar and S. K. Sahoo, *J. Photochem. Photobiol., A*, 2023, **437**, 114465.
42 A. Thangaraj, V. Bhardwaj and S. K. Sahoo, *Photochem. Photobiol. Sci.*, 2019, **18**, 1533–1539.
43 V. Bhardwaj, L. Hindocha, S. K. A. Kumar and S. K. Sahoo, *New J. Chem.*, 2022, **46**, 3248–3257.